Energy Reports 11 (2024) 2360–2373

Contents lists available at ScienceDirect

Energy Reports

journal homepage: www.elsevier.com/locate/egyr

Research paper

# Cooperative operational planning of multi-microgrid distribution systems with a case study

Ali Azizivahed [a], Khalil Gholami [b], Gloria V. Rupf [c], Ali Arefi [c], Christopher Lund [c], Jagpreet Walia [c], Md. Moktadir Rahman [d], Md. Rabiul Islam [e], SM. Muyeen [f], Innocent Kamwa [g,*]

[a] School of Electrical and Data Engineering, University of Technology Sydney, Sydney, Australia
[b] Renewable Energy and Electric Vehicle (REEV) Lab, School of Engineering, Deakin University, Geelong, VIC 3216, Australia
[c] School of Engineering and Energy, Murdoch University, Perth 6150, Australia
[d] Essential Energy, Port Macquarie, New South Wales 2444, Australia
[e] School of Electrical, Computer and Telecommunications Engineering, University of Wollongong, New South Wales 2522, Australia
[f] Electrical Engineering Department, Qatar University, Qatar
[g] Department of Electrical Engineering and Computer Engineering, Laval University, Quebec, QC G1V 0A6, Canada

ARTICLE INFO

*Keywords:*
Data clustering
Load profile grouping
Cooperative planning
Multi microgrid systems
Operation and planning

ABSTRACT

Clustering historical electricity consumption data is very important for creating representative demand profiles for the planning and operation of the power grids. This paper investigates a multi-dimensional framework for data clustering, which takes scattering and separation metrics, as well as the number of clusters into account. A combination of wavelet mutation with the Invasive Weed Optimization (IWO) method for clustering features is proposed. One notable advantage of the IWO method over other metaheuristic optimization algorithms is its ability to dynamically adapt the number of weed colonies during the search process, resulting in improved exploration and exploitation of the search space. The proposed strategy is applied to cluster the electricity consumption data from a large municipal government center in Perth, Western Australia. The suggested method is then evaluated by comparing it with the well-known method in the literature, namely, the k-means technique. After the data clustering, the obtained results are implemented in the design of a multi-microgrid system under two different scenarios of cooperative and noncooperative modes. To evaluate the performance of the proposed method, the proposed method is implemented on the operational planning of a real multi-microgrid distribution system in Western Australia using linear programming to take the advantage of the mathematical-based solvers. After performing some investigations, the cooperative mechanism, where the microgrids have participated in supplying the demand of microgrids was found to yield to greater operational and investment cost minimzation. In terms of numerical comparison, the total cost in the cooperative model is 6.5% lower than that in a non-cooperative situation.

## 1. Introduction

Microgrids, which come in diverse capacities and capabilities, have evolved into indispensable components of distribution networks. While some microgrids prioritize flexibility, others focus on energy storage and the integration of renewable energy sources (Gholami and Jazebi, 2020a). However, the true potential of microgrids lies in their ability to collaborate with one another, forming a multi-microgrid platform (Xu et al., 2018). This coordination of multiple microgrids offers a unique opportunity to maximize the advantages of each microgrid and enhance the overall efficiency and cost-effectiveness of the system. When multiple microgrids work in unison within a network, they can harness their unique strengths to create a more flexible and resilient energy infrastructure. Collectively, these microgrids can optimize the utilization of renewable resources, enhance grid stability, and adapt to changing energy demands. Furthermore, this collaborative approach not only benefits individual microgrids but also enhances the sustainability and reliability of the entire distribution network.

Besides, increasing energy prices, the threat of climate change and corporate environmental sustainability aims have prompted numerous corporate, institutional, and public organizations to place greater emphasis on regulating energy consumption and supply on their side of the municipal power grid. The power systems of such organizations can

* Corresponding author.
*E-mail address:* innocent.kamwa@gel.ulaval.ca (I. Kamwa).

https://doi.org/10.1016/j.egyr.2024.01.071
Received 6 July 2023; Received in revised form 3 November 2023; Accepted 28 January 2024
Available online 9 February 2024

**Nomenclature**

$\Theta C$ the decision-variables vector, which denotes the set of observations for cluster centriods
$N_{ob}$ the number of metrics and
$k^{th}$ the weighting of $k^{th}$ metric ($Mrt_k$). The weighting of the factors will depend on the decision- maker's point of view
$N_{cltr}$ and $\aleph_i$ Respectively, the number of clusters and observations in the $i^{th}$ cluster, respectively
$a_{i,n}$ the $n^{th}$ observation in the $i^{th}$ cluster
$c_i$ the centroid of the $i^{th}$ cluster.
$S_i$ and $\overline{S}_i$ the square mean of the Euclidean distance between each observation and the normalized form of it, respectively
$Mrt_1$ the first metric obtained by the scattering rate of observations within each cluster
$D_{i,j}$ the Euclidean distance reversal of the $i^{th}$ and the $j^{th}$ clusters
$\overline{D}_{i,j}$ it is obtained by dividing $D_{i,j}$ by the maximum Euclidean distance reversal through clusters to give the normalized value of $D_{i,j}$
$\mathscr{M}_i$ the maximum value of $\overline{D}_{i,j}$ for the $i^{th}$ and the $j^{th}$ clusters; and
$Mrt_2$ the second metric obtained from the mean of $\mathscr{M}_i$
$N_{cltr}^{\max}$ and $N_{cltr}^{\min}$ the maximum and the minimum number of clusters
$S_{\max}$ and $S_{\min}$ the predetermined maximum and minimum number of produced seeds, respectively
$OF^{best}$ and $OF^{worst}$ the fitness functions of the best and worst population, respectively
$S_p$ and $OF_p$ the number of seeds generated by the $p^{th}$ seed and the amount of fitness functions for the $p^{th}$ population
$\sigma^{itr}$ the standard deviation at $itr^{th}$ iteration;;; and $\alpha$ is the nonlinear modulation index
$itr^{\max}$ the maximum user-defined iteration
$\sigma^{final}$ and $\sigma^{initial}$ the final and initial standard deviations, respectively
$p^{th}$ and $q^{th}$ randomly chosen weed and its $q^{th}$ element that will go through wavelet mutation at the ith iteration within the sorted population
$\Theta C_q^{\max}$ and $\Theta C_q^{\min}$ respectively show the upper and lower bounds of for the $q^{th}$ component of the decision-variable vectors
$\sigma$ is the mother wavelet
$r$ a random integer produced from [− 2.5 h 2.5 h]
$h$ and $h^{\max}$ the dilation parameter and its maximum limit (i.e., $h^{\max}$= 10,000), respectively
$t$ the intervals of scheduling every hour $\in \boldsymbol{\Omega_T}$
$n, m$ the indexes of microgrid ($\in \boldsymbol{N_{MG}}$)
$i, j$ the indexes of network nodes ($\in \boldsymbol{N_{node}}$)
$\varrho_{expense}^{DNO}$ and $\varrho_{expense}^{MG}$ the cost associated with the distribution system operator (DSO) and microgrids, respectively;
$\Psi_{sub}^t$ and $\Psi_{MG}^{t,n}$ the price of energy at substation at $t^{th}$ hour and the price of energy exchange of $n^{th}$ microgrid at $t^{th}$ hour, respectively;
$P_{sub}^t$ the substation's real power during $t^{th}$ hour $\in \boldsymbol{P_{sub}}$;
$P_{n,m}^t$ the active power exchange from $n^{th}$ microgrid to $m^{th}$ microgrid at $t^{th}$ hour $\in \boldsymbol{P_{EEMG}^t}$;
$P_{demand}^t$ the system's power consumption at $t^{th}$hour
$P_{loss}^t$ the system's power went out in the $t^{th}$ hour
$\boldsymbol{P_{EEMG}^t}$ a set of microgrids' power exchanges during the $t^{th}$ hour $\in \boldsymbol{P_{EEMG}}$
$P_{PV}^{n,t}$ the electricity generated by $n^{th}$ PV at $t^{th}$ *hour*
$P_{BATch}$ and $P_{BATdis}$ the power of charge and discharge of the $n^{th}$ battery at $t^{th}$ hour
$OC_{DER}^n$ the operating cost for renewable sources of energy for $n^{th}$ microgrid
$OC_{BAT}^{n,t}$ the cost of operating the battery for $n^{th}$ microgrid at $t^{th}$ hour
$\xi_M^{PV}$ the investment cost for PV panels for maintenance and repairs over a year
$\Psi_{PV}^n$ PV panel investment rate in $n^{th}$ microgrid
$P_{PV}^{Size,n}$ PV panel size in $n^{th}$ microgrid
$\Psi_{cyc}^n$ the cost of cycling battery in $n^{th}$microgrid
$\beta^{n,t}$ the binary variable indicates the charge and discharge states of the battery of $n^{th}$ microgrid at $t^{th}$ hour $\in \beta^t$;
$P_{BAT_{ch}}^{n,t}$ and $P_{BAT_{dis}}^{n,t}$ the charging and discharging rates of the battery in $n^{th}$ microgrid at $t^{th}$ hour, respecyovely
$P_{ch}^{\max}$ and $P_{dis}^{\max}$ the maximum charging and discharge rates of the battery in $n^{th}$ microgrid at $t^{th}$ hour, respectively
$\rho_{ch}$ and $\rho_{dis}$ the efficiency of the charge/discharge process, respectively
$SOC^{n,t}$ the state of charges of the battery in $n^{th}$ microgrid at $t^{th}$ hour
$SOC^{\min}$ and $SOC^{\max}$; allowable ranges of state of harges of the battery
$SOC^{n,\Omega_T}$ and $SOC^{n,0}$ the SOC of the battery at the final and initial hours of scheduling, respectively
$\aleph_{ES}$ the maximum operation of charges and discharges of the battery over the time frame
$P_{D,i}^t$ and $Q_{D,i}^t$ the real and reactive electricity demands at $i^{th}$ node at $t^{th}$ hour, respectively
$P_{G,i}^t$ and $Q_{G,i}^t$ the real and reactive electricity generations at $i^{th}$ node at $t^{th}$ hour, respectively
$V_{sub}$ the voltage on the substation, (i.e., =1p.u.);
$V_{real,i}^t$ and $V_{img,i}^t$ the part of the real and imaginary voltages of $i^{th}$ node at $t^{th}$ hour, respectively
$I_{real,i}^t$and $I_{img,i}^t$ the part of the real and imaginary nodal current injection of $i^{th}$ node of the network at $t^{th}$ hour, respectively
$I_{real,(i,j)}^t$ and $I_{img,(i,j)}^t$ the art of the real and imaginary branch current between $i^{th}$ and $j^{th}$ nodes at $t^{th}$ hour, respectively
$g_{i,j}$ and $b_{i,j}$ the line conductance and susceptance between the $i^{th}$ and $j^{th}$ nodes, respectively
$N_{node}$ the total number of nodes of the network
$V^{\max}$ and $V^{\min}$ the boundaries of node voltages
$I_{(i,j)}^{\max}$ the maximum current capacity of the line between $i^{th}$ and $j^{th}$ nodes
$\mathscr{T}_{(.)}$ a set of the specified continuous range's discretization $(-(), +())$, $() = V^{\max}, I_{(i,j)}^{\max}$

be controlled as a (virtual) microgrid, with dispersed forms of distributed resources (e.g., renewable sources, batteries) and loads that are operating parallel to the main grid. Organizations would be able to properly monitor and regulate their energy usage and generation (from renewables and batteries) through the application of a long-term virtual microgrid planning algorithm (Azizivahed et al., 2020). Identification and measurement of the consumption and generation patterns at an organization's facilities are the foundational step to devising a robust planning framework. Limiting demand uncertainty by creating indicative demand profiles for facilities that accurately capture the features of load profiles can lead to more cost-effective long-term network planning (Arefi et al., 2016). Electricity demand can be characterized through

clustering, which enables representative load profile groups to be created (McLoughlin et al., 2015). The research outlined in (McLoughlin et al., 2015) found the self-organizing maps (SOM) clustering approach to be among the most successful for dividing residential electricity consumption datasets into load profile groups without missing distinctive data related to the load profile shape. For peak-valley analysis and predicting average consumption and power loss for planning, one study (Deepak Sharma and Singh, 2014) employed the k-means clustering technique to group comparable load profiles within different zones. Clustering of historical load profile data has also been employed for load profile analysis to customize energy retail pricing for residential customers (Yang et al., 2019). Alternative clustering algorithms to k-means and SOM that have been used for load profile analysis include flexible k-means, hierarchical, finite mixture model, fuzzy c-means, support vector, two-stage with fast wavelet transformation (FWT) and g-means, and subspace project method based clustering, as well as clustering by fast search and find of density peaks (Kwac et al., 2014; Li et al., 2015; Haben et al., 2016; Zhang et al., 2012; Chicco and Ilie, 2009; Mets et al., 2016; Piao et al., 2014; Wang et al., 2016; Narimani et al., 2019). The focus of these clustering algorithms, however, has been on either increasing cluster separation or minimizing the dispersion of members within a group. Those methods that do consider both factors do not take them into account as a multi-objective to enable decision-makers to emphasize the characteristic that best fits their case or analysis.

Considering this fact that, the proposed formulation seeks the optimal solution, eg., the best clustering with the least members but more accurate, an optimization approach is essential. There are various optimization tools. For example, in reference, the authors developed a heuristic approach to clustering the data just by considering the centroid of clusters (Gholami et al., 2022a). However, a unique hybridized method to optimize the clustering objective function using both Invasive Weed Optimization (IWO) and wavelet mutation strategy is provided in this paper (Azizivahed et al., 2021a). The IWO mimics the behavior of colonizing weeds and can locate desired minima quickly (Mehrabian and Lucas, 2006). The outcomes of implementing this proposed methodology to metered consumption data from the Civic Centre of a large local government (municipality), in Perth, Western Australia (WA) are also presented. The test facility is an administrative building, which is comparable to a commercial office building. Comparisons of each seasonal cluster utilizing the innovative clustering strategy with ones created through the well-known k-means and original IWO approaches are made using Davies-Bouldin and silhouette indices (Arbelaitz et al., 2013).

Microgrids are emerging energy systems that may be operated under both grid-connected and islanded modes. In terms of grid-connected situation, they are able to trade power with the upstream network. This mode is excellent for areas with consistent grid connection. Microgrids, on the other hand, may function in an isolated mode, operating autonomously of the primary grid and producing, storing, and controlling the electricity they require (Gholami and Jazebi, 2020b). With regard to the plan of microgrids, some investigations have been done so far. For example, authors of (Gholami et al., 2022b) developed an optimization approach for optimal economic dispatch of islanded networked microgrids (MGs) integrated with thermal and renewable resources. Due to the fact that islanded MGs are under high penetration of renewable resources, using energy storage in the presence of such resources is inevitable. As a result, researchers in (Zhang et al., 2016) developed a bi-level approach for the planning of islanded MGs, where the upper level tries to identify the sizing of resources (renewables and energy storages), but the dispatch of these resources is done at lower level. In order to make the model much more realistic, the uncertainties with resources in MGs that are operated in both mentioned modes were investigated in (Khodaei et al., 2015), (Narayan and Ponnambalam, 2017). In more detail, a team of researchers in (Narayan and Ponnambalam, 2017) devised a stochastic planning method for optimizing the allocation of resources within islanded microgrids. Their primary objective was to mitigate the planning risk by integrating considerations related to the uncertainties associated with renewable energy resources. Besides, Authors of (Mina-Casaran et al., 2021) concentrated on the incorporating demand response programming in the planning of microgrids. In deeper explanation, they developed a planning approach for optimal sizing of DERs in microgrids under considering demand side management as well. The model was a bi-level programming, where the investment was calculated in upper level while the lower level solves the operation part of sized resources. The study in (Contreras et al., 2019) explored the microgrid planning within a multi-objective framework. To address this complex task, the researchers applied the non-dominated sorting genetic algorithm II (NSGA-II) to efficiently handle the challenges associated with microgrid planning, particularly in minimizing power balance discrepancies in islanded mode. An intriguing aspect of this research lies in its use of a multi-objective approach. However, it's worth noting that the reliance on heuristic methods in this approach might not ensure the attainment of a globally optimal solution. A research in (Shawon et al., 2023) focused on the first phases of microgrid design by the strategic placement and size of DGs to reduce energy losses by directly delivering electricity to local loads. In other words, it presents a non-linear programming (NLP) approach for DG placement that approaches planning as AC optimum power flow (OPF) equations. The efficacy of the strategy is proven using both an IEEE 33-bus test system and a genuine 404-bus distribution system run by Saskatoon Light and Power in Canada. Importantly, in terms of performance, the suggested strategy outperforms previous alternatives. However, the model was nonlinear because of AC power flow equations as well as the collaboration between microgrids have not been investigated. Accordingly, the linear load flow is still essential to have accurate and promising solutions. According to the aforementioned papers, it is clear that a multi-microgrid system was designed without collaboration among them. Consequently, we still need to develop a planning approach for the simultaneous planning of multi-microgrid systems considering the collaboration between MGs and the upstream grid.

The clustered data is also used to present a concept for electricity trading of MGs, specifically where certain MGs are controlled by an organization, using a case study of a local government in WA. In the developed framework, MGs can start trading electricity within and between themselves. Trading would occur between MGs and facilities within MGs that have excess production (from distributed energy resources such as renewables and batteries) and other MGs and facilities that do not have enough production to satisfy the demands. However, MGs would be expected to pay for the use of the distribution system, referred to as network charge, as well as their share of network loss as a result of the energy transactions. Network loss is considered and estimated in the framework by using an efficient load flow. The proposed method is then tested on a multi-microgrid system in WA under two conditions, cooperation among MGs (active participation in the electricity exchange between each other) and non-collaborative (interaction with the grid only and not between MGs). The main contributions of this paper are as follows.

- This study, which launched a sophisticated clustering method, separates historical data into groupings. This effective division not only organizes the data but also considerably reduces the computing strain, increasing data processing efficiency.
- The article advances the discipline of power system analysis by presenting a unique approach for precisely calculating network losses resulting from energy transactions. This approach, which is based on an effective and linear power flow model, offers an improved awareness of how energy exchange affects network performance.
- The study provides a two methodologies for developing distributed multi-microgrid systems. In the first scenario, each microgrid individually satisfies its load demands in a noncooperative setting. In the second scenario, power is bought and sold by microgrids as part of the collaboration. The advantages of cooperative microgrid

operation in terms of resource optimization are shown by analysis of these cases.

- The study's real evidence of decreased operating and investment expenses is one of its most persuasive features. Implementing the suggested structure, which skillfully combines energy storage and renewable energy sources within microgrids, results in significant cost reductions. These cost savings highlight the move to microgrid systems that are more robust and sustainable.

## 2. Planning of multi-microgrid distribution system

### 2.1. Problem visualization

A mathematical-based optimization problem is used to describe how a distribution network with many private MGs operates. To have a distinct overview on the model, Fig. 1 illustrates the architectural diagram of the proposed multi-microgrid distribution system. The distribution network operator (DSO) monitors power exchange with the upstream network and energy exchange between MGs. In addition, each microgrid makes an effort to enhance its benefit or decrease its operational cost at the lowest level (Azizivahed et al., 2021b).

### 2.2. Objective function and constraints

In the DSO level, the distribution system operator organizes the power trading between MGs and between the grid and MGs. Following is a definition of the system's (all sites and the network's) objective function. Equation (01a) represents the objective function, encompassing the cost components of utility, energy transaction between Microgrids (MGs), and maintenance costs for Battery Energy Storage Systems (BESS) and Photovoltaic (PV) systems. Equations (01b) and (01c) define the energy flow from one MG to another and establish the power balance across the entire network. Furthermore, Equations (01d) and (01e) detail the operation and maintenance costs associated with PV systems and BESS. Equations (01 f) to (01k) are dedicated to the operational constraints governing battery behavior, including the maximum and minimum state-of-charge (SOC), charge/discharge rates, and limitations on transitions between charging and discharging (Gholami et al., 2023). These constraints are crucial in prolonging BESS lifespan while ensuring efficient system performance.

$$\min_{\mu_{DSO},\mu_{MG}} \left[ \varrho^{DSO}_{expense} + \varrho^{MG}_{expense} \right]$$

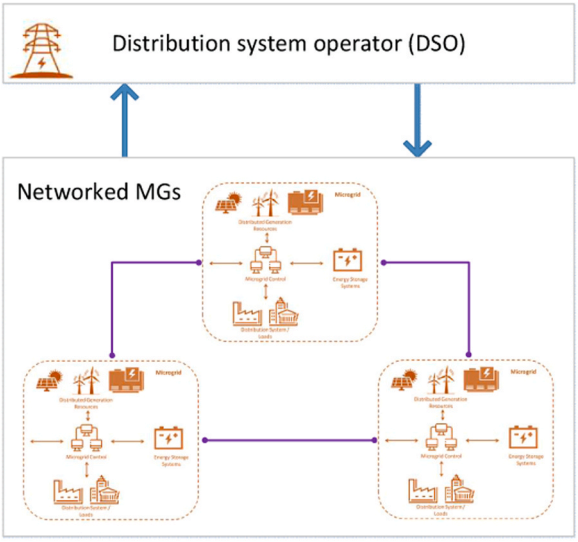


**Fig. 1.** A visual representation of a multi-microgrid distribution system.

$$\varrho^{DSO}_{expense} = \sum_{t\in\Omega_T} \left( \Psi^{t}_{sub} P^{t}_{sub} + \sum_{m\in N_{MG}} \sum_{m\neq n\in N_{MG}} \Psi^{t,n}_{MG} \left( P^{t}_{n,m} \right)^{+} \right)$$

$$\varrho^{MG}_{expense} = \sum_{n\in N_{MG}} OC^{n}_{DER} + \sum_{t\in\Omega_T} \sum_{n\in N_{MG}} OC^{n,t}_{BAT} \tag{01a}$$

*s.t.*

$$\left( P^{t}_{n,m} \right)^{+} = \max\left( 0, P^{t}_{n,m} \right) \tag{01b}$$

$$P^{t}_{sub} = P^{t}_{demand} + P^{t}_{loss} + \sum_{n\in N_{MG}} \left( P^{n,t}_{BAT_{ch}} - P^{n,t}_{BAT_{dis}} - P^{n,t}_{PV} \right) \tag{01c}$$

$$OC^{n}_{DER} = \left( \xi^{PV}_{M} \Psi^{n}_{PV} P^{Size,n}_{PV} \right) / 365, \forall n \tag{01d}$$

$$OC^{n,t}_{BAT} = \Psi^{n}_{cyc} \left| \beta^{n,t} - \beta^{n,t-1} \right|, \forall t, n \tag{01e}$$

$$0 \le P^{n,t}_{BAT_{ch}} \le P^{\max}_{ch} \quad \beta^{t}, \forall t, n \tag{01 f}$$

$$0 \le P^{n,t}_{BAT_{dis}} \le P^{\max}_{dis} (1 - \beta^{n,t}), \forall t, n \tag{01 g}$$

$$SOC^{n,t} = SOC^{n,t-1} + \rho_{ch} P^{n,t}_{BAT_{ch}} - P^{n,t}_{BAT_{dis}} / \rho_{dis}, \forall t, n \tag{01 h}$$

$$SOC^{\min} \le SOC^{n,t} \le SOC^{\max}, \forall t, n \tag{01i}$$

$$SOC^{n,\Omega_T} = SOC^{n,0}, \forall t, n \tag{01j}$$

$$\sum_{t=2}^{\Omega_T} \left| \beta^{n,t} - \beta^{n,t-1} \right| \le \aleph_{BAT}, \forall n \tag{01k}$$

and: power flow constraints which are discussed as follows· (01 l)

where, $t$ indicates the intervals of scheduling every hour $\in \boldsymbol{\Omega_T}$; $n, m$ and $i, j$ are, respectively, the indexes of microgrid ($\in N_{MG}$) and network nodes ($\in N_{node}$); $\varrho^{DNO}_{expense}$ and $\varrho^{MG}_{expense}$ signify the cost associated with the distribution system operator (DSO) and microgrids, respectively; $\Psi^{t}_{sub}$ and $\Psi^{t,n}_{MG}$ denote the price of energy at substation at $t^{th}$ hour and the price of energy exchange of $n^{th}$ microgrid at $t^{th}$ hour, respectively; $P^{t}_{sub}$ demonstrates the substation's real power during $t^{th}$ hour $\in \boldsymbol{P}_{sub}$; $P^{t}_{n,m}$ shows the active power exchange from $n^{th}$ microgrid to $m^{th}$ microgrid at $t^{th}$ hour $\in \boldsymbol{P}^{t}_{EEMG}$; $P^{t}_{demand}$ is the system's power consumption at $t^{th}$hour; $P^{t}_{loss}$ the system's power went out in the $t^{th}$ hour; $\boldsymbol{P}^{t}_{EEMG}$ is a set of microgrids' power exchanges during the $t^{th}$ hour $\in \boldsymbol{P}_{EEMG}$; $P^{n,t}_{PV}$ the electricity generated by $n^{th}$ PV at $t^{th}$; $P_{BATch}$ and $P_{BATdis}$ illustrates the power of charge and discharge of the $n^{th}$ battery at $t^{th}$ hour; $OC^{n}_{DER}$ denotes the operating cost for renewable sources of energy for $n^{th}$ microgrid; and $OC^{n,t}_{BAT}$ demonstrates the cost of operating the battery for $n^{th}$ microgrid at $t^{th}$ hour. $\xi^{PV}_{M}$ is the investment cost for PV panels for maintenance and repairs over a year; $\Psi^{n}_{PV}$ shows PV panel investment rate in $n^{th}$ microgrid; $P^{Size,n}_{PV}$ PV panel size in $n^{th}$ microgrid; $\Psi^{n}_{cyc}$ demonstrates the cost of cycling battery in $n^{th}$microgrid; $\beta^{n,t}$ illustrates the binary variable indicates the charge and discharge states of the battery of $n^{th}$ microgrid at $t^{th}$ hour $\in \beta^{t}$; $P^{n,t}_{BAT_{ch}}$ and $P^{n,t}_{BAT_{dis}}$ are respectively the charging and discharging rates of the battery in $n^{th}$ microgrid at $t^{th}$ hour; $P^{\max}_{ch}$ and $P^{\max}_{dis}$ represent the maximum charging and discharge rates of the battery in $n^{th}$ microgrid at $t^{th}$ hour; $\rho_{ch}$ and $\rho_{dis}$ are the efficiency of the charge/discharge process, respectively; $SOC^{n,t}$ is the state of charges of the battery in $n^{th}$ microgrid at $t^{th}$ hour which is kept between allowable ranges by $SOC^{\min}$ and $SOC^{\max}$; $SOC^{n,\Omega_T}$ and $SOC^{n,0}$ represent the SOC of

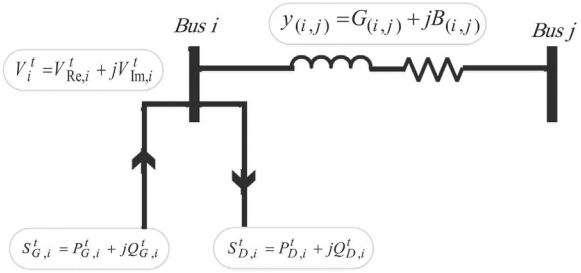


**Fig. 2.** A simple network for KCL concept.

the battery at the final and initial hours of scheduling; and $\mathsf{N}_{ES}$ shows the maximum operation of charges and discharges of the battery over the time frame.

The constraints and restrictions of the systems are addressed using the AC power flow formulas.The following KCL equations belong to Fig. 2, where the load flow is represented

$$2P_{D,i}^t - P_{G,i}^t \approx \frac{P_{D,i}^t}{V_{sub}} V_{real,i}^t - \frac{Q_{D,i}^t}{V_{sub}} V_{img,i}^t - V_{sub} I_{real,i}^t, \forall i, t \tag{02a}$$

$$2Q_{D,i}^t - Q_{G,i}^t \approx \frac{Q_{D,i}^t}{V_{sub}} V_{real,i}^t - \frac{P_{D,i}^t}{V_{sub}} V_{img,i}^t + V_{sub} I_{img,i}^t, \forall i, t \tag{02b}$$

here $P_{D,i}^t$ and $Q_{D,i}^t$ represent the real and reactive electricity demands at $i^{th}$ node at $t^{th}$ hour, respectively; $P_{G,i}^t$ and $Q_{G,i}^t$ denote the real and reactive electricity generations at $i^{th}$ node at $t^{th}$ hour, respectively; $V_{sub}$ is the voltage on the substation, (i.e., =1p.u.); $V_{real,i}^t$ and $V_{img,i}^t$ respectively signify the part of the real and imaginary voltages of $i^{th}$ node at $t^{th}$ hour; $I_{real,i}^t$and $I_{img,i}^t$ respectively demonstrate the part of the real and imaginary nodal current injection of $i^{th}$ node of the network at $t^{th}$ hour; $I_{real,(i,j)}^t$ and $I_{img,(i,j)}^t$ are respectively the art of the real and imaginary branch current between $i^{th}$ and $j^{th}$ nodes at $t^{th}$ hour;.

The aforementioned KCL equations can be approximated linearly using the second order of Taylor expansion. The real and imaginary components of the KVL equations are separated as follows:

$$I_{real,i}^t = \sum_{j \in N_{node}} G_{i,j} V_{real,i}^t - \sum_{j \in N_{node}} B_{i,j} V_{img,i}^t \tag{03a}$$

$$I_{img,i}^t = \sum_{j \in N_{node}} G_{i,j} V_{img,i}^t + \sum_{j \in N_{node}} B_{i,j} V_{real,i}^t \tag{03b}$$

where $g_{i,j}$ and $b_{i,j}$ show the line conductance and susceptance between the $i^{th}$ and $j^{th}$ nodes, respectively; the total number of nodes of the network is also expressed by $N_{node}$.

The voltage and current constraints:

$$(V^{\min})^2 \le \left(V_{real,j}^t\right)^2 + \left(V_{img,j}^t\right)^2 \le (V^{\max})^2 \tag{04a}$$

$$\left(I_{real,(i,j)}^t\right)^2 + \left(I_{img,(i,j)}^t\right)^2 \le \left(I_{(i,j)}^{\max}\right)^2 \tag{04b}$$

$$I_{real,(i,j)}^t = g_{i,j}\left(V_{real,i}^t - V_{real,j}^t\right) - b_{i,j}\left(V_{img,i}^t - V_{img,j}^t\right) \tag{04c}$$

$$I_{img,(i,j)}^t = g_{i,j}\left(V_{img,i}^t - V_{img,j}^t\right) + b_{i,j}\left(V_{real,i}^t - V_{real,j}^t\right) \tag{04d}$$

in the above expressions, $V^{\max}$ and $V^{\min}$ are the boundaries of node voltages; and $I_{(i,j)}^{\max}$ guarantees the maximum current capacity of the line between $i^{th}$ and $j^{th}$ nodes would not be rebelled.

Finally, the hexagon linear approximation is deployed to linearize the mentioned equations (Gholami et al., 2022c):

$$\left|V_{img,i}^t\right| \le \frac{-\zeta V_{real,i}^t + (V^{\max})^2}{\sqrt{(V^{\max})^2 - \zeta^2}}, \forall t, i, \forall \zeta \in \mathscr{T}_{V^{\max}} \tag{05a}$$

$$V^{\min} \le V_{real,i}^t, \forall i, t \tag{05b}$$

$$\left|I_{img,(i,j)}^t\right| \le \frac{-\zeta I_{real,(i,j)}^t + \left(I_{(i,j)}^{\max}\right)^2}{\sqrt{\left(I_{(i,j)}^{\max}\right)^2 - \zeta^2}}, \forall t, (i,j), \forall \zeta \in \mathscr{T}_{I_{(i,j)}^{\max}} \tag{05c}$$

Here $\mathscr{T}_{(.)}$ **is** a set of the specified continuous range's discretization $(-(), +())$, $() = V^{\max}, I_{(i,j)}^{\max}$;.

The amount of generation and demand of each node of the network is:

$$P_i^D = P_{demand}^{i,t} \forall i \in N_{MG} \tag{06a}$$

$$Q_{D,i}^t = P_{D,i}^t \tan(\varphi_i) \forall i \in N_{node} \tag{06b}$$

$$P_{G,i}^t = P_{PV}^{i,t} + P_{BAT_{dis}}^{i,t} - P_{BAT_{ch}}^{i,t} + \sum_{m \in N_{MG}\ m \ne i} \left(\left(P_{i,m}^t\right)^- - \left(P_{i,m}^t\right)^+\right) \forall i \in N_{MG} \tag{06c}$$

$$Q_{G,i}^t = P_{G,i}^t \tan(\varphi_i) \forall i \in N_{node} \tag{06d}$$

$$\left(P_{i,m}^t\right)^- = \min\left(0, P_{i,m}^t\right) \forall i \in N_{node} \tag{06e}$$

In the suggested formulation, the equation of power loss has linear nature as given:

$$P_{loss}^t = V_{sub} I_{sub}^{real} + \sum_{n \in N_{MG}} \left(P_{PV}^{n,t} + P_{BAT_{dis}}^{n,t} - P_{BAT_{ch}}^{n,t}\right) - \sum_{j \in N_{node}} P_{demand}^{j,t} \quad , \forall t \tag{07a}$$

Problem decision variables.

The decision variables vector of the proposed problem consists of the variables controlled by the DSO and each MGs separately.

DSO:

$$\mu_{DSO} = [P_{sub}, P_{EEMG}, (P_{EEMG})^+] \tag{08a}$$

$$P_{sub} = \left(P_{sub}^t, \forall t \in \Omega_T\right) \tag{08b}$$

$$P_{sub}^t = \left[P_{sub}^{1,t} \quad P_{sub}^{2,t} \quad \dots \quad P_{sub}^{N,t}\right], \forall t \in \Omega_T \tag{08c}$$

$$P_{EEMG} = \left(P_{EEMG}^t, \forall t \in \Omega_T\right) \tag{08d}$$

$$P_{EEMG}^t = \left(P_{n,m}^t, \forall n \in N_{MG}, \forall m \in N_{MG}\right), \forall t \tag{08e}$$

$$P_{n,n}^t = 0, \forall t, n \tag{08 f}$$

$$P_{m,n}^t = -P_{n,m}^t, \forall t, m, n \tag{08 g}$$

$$(P_{EEMG}^t)^+ = \left(\left(P_{n,m}^t\right)^+, \forall n \in N_{MG}, \forall m \in N_{MG}\right), \forall t \tag{08 h}$$

MG:

$$\mu_{MG} = \left[P_{BAT_{ch}}, P_{BAT_{dis}}, \beta\right] \tag{08i}$$

$$P_{BAT_{ch}} = \left(P_{BAT_{ch}}^t, \forall t \in \Omega_T\right) \tag{08j}$$

$$P_{BAT_{ch}}^t = \left[P_{BAT_{ch}}^{1,t}, P_{BAT_{ch}}^{2,t}, \dots, P_{BAT_{ch}}^{N,t}\right] \tag{08k}$$

$$P_{BAT_{dis}} = \left(P_{BAT_{dis}}^t, \forall t \in \Omega_T\right) \tag{08 l}$$

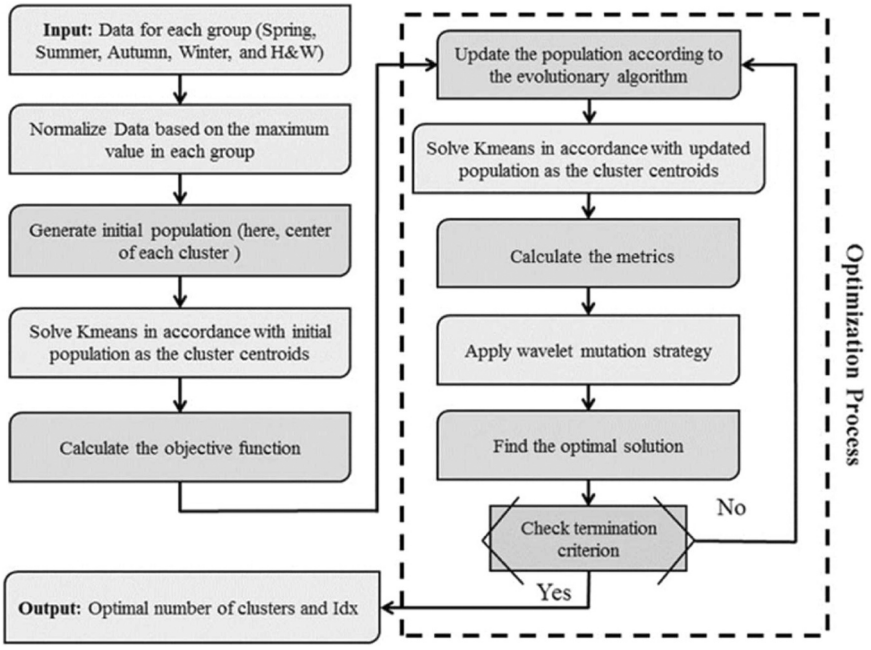


**Fig. 3.** The flowchart detailing the process of data clustering using the modified Invasive Weed Optimization (IWO) algorithm.

$$P^{t}_{BAT_{dis}} = \left[P^{1,t}_{BAT_{dis}}, P^{2,t}_{BAT_{dis}}, \ldots, P^{N,t}_{BAT_{dis}}\right] \quad (08\,\mathrm{m})$$

$$\beta = (\beta^{t}, \forall t \in \Omega_{T}) \quad (08\mathrm{n})$$

$$\beta^{t} = \left[\beta^{1,t}, \beta^{2,t}, \ldots, \beta^{N,t}\right] \quad (08\mathrm{o})$$

## 3. Data clustering

As mentioned previously, this paper is in aiming to develop an optimization approach for a real-case study in WA, Australia. In this regard, the project is developed according to a long-term historical data (demand in particluar) from several sites in a same area. Toward this end, an efficient clustering approach is developed to organize the historical data to make the project more reflective.

In this section, three different metrics are introduced to increase the clustering quality in terms of scattering within clusters, differentiation between clusters, and the number of clusters, which can be very important in some special cases. Some well-known indices (Arbelaitz et al., 2013) combine scattering within clusters and the separation between clusters into a single metric. As a result, multiple weighted-sum factors to change the priority of any metric cannot be applied. Therefore, the metrics are split in order to enable their priorities to be adjusted through different weight factors. The proposed metrics are detailed in depth in the next section.

### 3.1. A. Metrics

The main metric (Mrt) for enhancing clustering quality is calculated by adding the normalized values of each discrete objective function with consideration of the weight factors.

$$\mathrm{Min}_{\Theta C}(Mrt) = \sum_{k=1}^{N_{ob}} \omega_{k} Mrt_{k} \quad (09a)$$

$$s.t. \sum_{k} \omega_{k} = 1 \quad (09b)$$

In the above equations, $\Theta C$ is the decision-variables vector, which denotes the set of observations for cluster centriods. In the optimization problem, the variable vector will be found based on minimizing the metrics, where $N_{ob}$ and $k^{th}$ are the number of metrics and the weighting of $k^{th}$ metric ($Mrt_{k}$). The weighting of the factors will depend on the decision-maker's point of view.

#### 3.1.1. Scattering metric

The scattering of observations in each cluster is represented by the following metric, $Mrt_{1}$. Each observation's Euclidean distance from the centroid of the assigned cluster is implemented. By minimizing the subsequent metric, the scattering rate will decrease. The scattering rate of observations within each cluster can be reduced by minimizing $Mrt_{1}$.

$$Mrt_{1} = \frac{1}{N_{cltr}} \sum_{i=1}^{N_{cltr}} \overline{S}_{i} \quad (10a)$$

$$s.t. \overline{S}_{i} = \frac{S_{i}}{\mathrm{Max}_{\forall j}(S_{j})} \quad (10b)$$

$$S_{i} = \sqrt{\frac{1}{\mathrm{N}_{i}} \sum_{n=1}^{\mathrm{N}_{i}} \left\| a_{i,n} - c_{i} \right\|} \quad (10c)$$

In this function, $N_{cltr}$ and $\mathrm{N}_{i}$ are the number of clusters and observations in the $i^{th}$ cluster, respectively; $a_{i,n}$ and $c_{i}$ signify the $n^{th}$ observation in the $i^{th}$ cluster, respectively; $S_{i}$ and $\overline{S}_{i}$ are the square mean of the Euclidean distance between each observation in the $i^{th}$ cluster and the centroid of the $i^{th}$ cluster and the normalized form of it, respectively; and the first objective function, $Mrt_{1}$, is the mean of $\overline{S}_{i}$.

#### 3.1.2. Separation metric

The separation of cluster centroids is indicated by the second metric. Euclidean distance is the main component of this metrics, which when minimized, will increase the separation rate of the clusters.

$$Mrt_{2} = \frac{1}{N_{cltr}} \sum_{i=1}^{N_{cltr}} \mathscr{M}_{i} \quad (11a)$$

$$s.t.\mathscr{M}_i = \mathrm{Max}_{\forall j, j\neq i}\left(\overline{D}_{i,j}\right) \tag{11b}$$

$$\overline{D}_{i,j} = \frac{D_{i,j}}{\mathrm{Max}_{\forall m,n;m\neq n}\left(D_{m,n}\right)} \tag{11c}$$

$$D_{i,j} = \frac{1}{\left\|c_i - c_j\right\|}, \forall i,j \tag{11d}$$

For this equation, $D_{i,j}$ is the Euclidean distance reversal of the $i^{th}$ and the $j^{th}$ clusters; $\overline{D}_{i,j}$ is obtained by dividing $D_{i,j}$ by the maximum Euclidean distance reversal through clusters to give the normalized value of $D_{i,j}$; $\mathscr{M}_i$ is the maximum value of $\overline{D}_{i,j}$ for the $i^{th}$ and the $j^{th}$ clusters; and $Mrt_2$ is the second metric obtained from the mean of $\mathscr{M}_i$. The quality of clustering will be enhanced by increasing the separation between clusters through the minimization of this metrics.

### 3.1.3. Number of clusters

The normalized form of the number of clusters is given by the third mertic. This metric is essential in a given problem to reduce its complexity and enable decision-makers to identify the dominating cluster more easily. Conversely, $Mrt_1$ tends to increase the number of clusters to reduce the scattering rate. In light of this, it is crucial to take this metric into account when solving this clustering problem. The normalized representation of the number of cluster is achieved using the fuzzy approach (Tran, 2004). The following is the defined metric's mathematical definition:

$$Mrt_3 = \frac{N_{cltr} - N_{cltr}^{\min}}{N_{cltr}^{\max} - N_{cltr}^{\min}} \tag{12a}$$

$$s.t. N_{cltr} = Size(Unique(\Theta C)) \tag{12b}$$

where $N_{cltr}^{\max}$ and $N_{cltr}^{\min}$ denote the maximum and the minimum number of clusters, respectively.

## 3.2. Optimization of the clustering

Clustering is an optimization problem with specific objective functions and decision variables, as previously mentioned. In terms of determining the centroid of each cluster, the optimal number of clusters, and clustering in line with a specific metric, k-means and traditional clustering algorithms have various drawbacks. Consequently, to identify the ideal number of clusters and the clusters' centroids in order to optimize the stated metric, the well-known meta-heuristic optimization algorithm called invasive weed optimization (IWO) is used. This method's superiority has been demonstrated in some engineering optimization problems, including data mining and image processing (Castillo et al., 2018). A modified IWO technique is also applied to the

**Table 1**
The Clustering Results based on the Developed Framework for the Spring Group under the various Scenarios.

| Scenarios | Weights | | | Objective Functions | | | Criterions | |
|---|---|---|---|---|---|---|---|---|
| | w1 | w2 | w3 | Ob1 | Ob2 | Ob3 | DBI | SI |
| 1 | 1 | 0 | 0 | 0.72 | 0.48 | 0.5 | 0.86 | 0.67 |
| 2 | 0 | 1 | 0 | 0.75 | 0.31 | 1 | 1.14 | 0.46 |
| 3 | 0 | 0 | 1 | 0.95 | 1 | 0 | 0.81 | 0.67 |
| 4 | 0.7 | 0.3 | 0 | 0.79 | 0.37 | 0.75 | 1.00 | 0.58 |
| 5 | 0.5 | 0.5 | 0 | 0.86 | 0.35 | 0.62 | 1.29 | 0.40 |
| 6 | 0.3 | 0.7 | 0 | 0.83 | 0.33 | 0.87 | 1.35 | 0.42 |
| 7 | 0.7 | 0 | 0.3 | 0.77 | 0.72 | 0.12 | 0.66 | 0.73 |
| 8 | 0.5 | 0 | 0.5 | 0.81 | 0.48 | 0.25 | 0.88 | 0.64 |
| 9 | 0.3 | 0 | 0.7 | 0.82 | 0.43 | 0.37 | 0.99 | 0.55 |
| 10 | 0 | 0.7 | 0.3 | 0.83 | 0.33 | 0.62 | 1.08 | 0.47 |
| 11 | 0 | 0.5 | 0.5 | 0.85 | 0.38 | 0.75 | 1.35 | 0.31 |
| 12 | 0 | 0.3 | 0.7 | 0.87 | 0.58 | 0.25 | 1.36 | 0.32 |
| 13 | $0.\overline{3}$ | $0.\overline{3}$ | $0.\overline{3}$ | 0.83 | 0.38 | 0.37 | 0.99 | 0.58 |

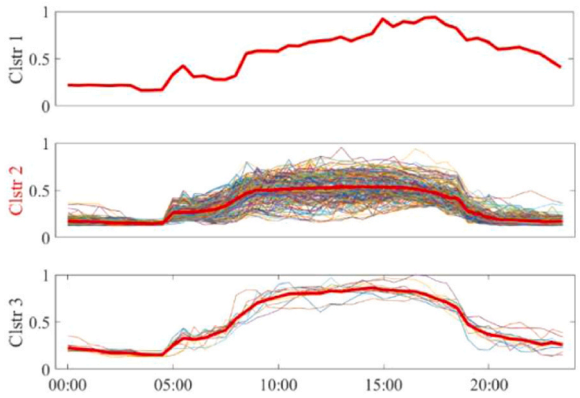


**Fig. 4.** The outcomes derived from the clustering technique developed for the spring group.

**Table 2**
Proportion of every Cluster for Different Seasons.

| Hybrid Approach | | | | | |
|---|---|---|---|---|---|
| Clusters | Spring | Summer | Autumn | Winter | H&W |
| 1 | 0.52 | 0.56 | 4.84 | 51.69 | 0.29 |
| 2 | 94.27 | 37.22 | 1.08 | 47.83 | 0.29 |
| 3 | 5.21 | 0.55 | 94.08 | 0.48 | 5.28 |
| 4 | - | 61.67 | - | - | 94.14 |

**Table 3**
The Clustering Results based on the Developed Framework for the Summer Group under the Various Scenarios.

| Scenarios | Weights | | | Objective Functions | | | Criterions | |
|---|---|---|---|---|---|---|---|---|
| | w1 | w2 | w3 | Ob1 | Ob2 | Ob3 | DBI | SI |
| 1 | 1 | 0 | 0 | 0.68 | 0.28 | 0.87 | 0.89 | 0.67 |
| 2 | 0 | 1 | 0 | 0.87 | 0.25 | 0.62 | 1.41 | 0.35 |
| 3 | 0 | 0 | 1 | 0.75 | 1 | 0 | 0.73 | 0.63 |
| 4 | 0.7 | 0.3 | 0 | 0.79 | 0.40 | 0.5 | 0.99 | 0.59 |
| 5 | 0.5 | 0.5 | 0 | 0.79 | 0.37 | 0.62 | 1.13 | 0.49 |
| 6 | 0.3 | 0.7 | 0 | 0.80 | 0.32 | 1 | 1.32 | 0.42 |
| 7 | 0.7 | 0 | 0.3 | 0.79 | 0.35 | 0.37 | 0.87 | 0.63 |
| 8 | 0.5 | 0 | 0.5 | 0.85 | 0.47 | 0.25 | 1.31 | 0.38 |
| 9 | 0.3 | 0 | 0.7 | 0.94 | 0.63 | 0.12 | 0.92 | 0.58 |
| 10 | 0 | 0.7 | 0.3 | 0.75 | 0.26 | 0.75 | 0.99 | 0.47 |
| 11 | 0 | 0.5 | 0.5 | 0.76 | 0.40 | 0.37 | 0.84 | 0.64 |
| 12 | 0 | 0.3 | 0.7 | 0.72 | 0.43 | 0.25 | 0.68 | 0.70 |
| 13 | $0.\overline{3}$ | $0.\overline{3}$ | $0.\overline{3}$ | 0.69 | 0.478 | 0.5 | 0.81 | 0.69 |

**Table 4**
The Clustering Results based on the Developed Framework for the Autumn Group.

| Scenarios | Weights | | | Objective Functions | | | Criterions | |
|---|---|---|---|---|---|---|---|---|
| | w1 | w2 | w3 | Ob1 | Ob2 | Ob3 | DBI | SI |
| 1 | 1 | 0 | 0 | 0.68 | 0.31 | 0.75 | 1.01 | 0.55 |
| 2 | 0 | 1 | 0 | 0.70 | 0.21 | 0.87 | 0.97 | 0.56 |
| 3 | 0 | 0 | 1 | 0.98 | 0.65 | 0.12 | 0.74 | 0.65 |
| 4 | 0.7 | 0.3 | 0 | 0.80 | 0.55 | 0.12 | 0.66 | 0.65 |
| 5 | 0.5 | 0.5 | 0 | 0.82 | 0.39 | 0.25 | 0.98 | 0.46 |
| 6 | 0.3 | 0.7 | 0 | 0.83 | 0.34 | 0.37 | 0.77 | 0.59 |
| 7 | 0.7 | 0 | 0.3 | 0.81 | 0.25 | 0.62 | 1.03 | 0.46 |
| 8 | 0.5 | 0 | 0.5 | 0.81 | 0.47 | 0.25 | 0.64 | 0.71 |
| 9 | 0.3 | 0 | 0.7 | 0.87 | 0.62 | 0.12 | 0.64 | 0.72 |
| 10 | 0 | 0.7 | 0.3 | 0.77 | 0.32 | 0.37 | 0.67 | 0.59 |
| 11 | 0 | 0.5 | 0.5 | 0.76 | 0.30 | 0.5 | 0.83 | 0.62 |
| 12 | 0 | 0.3 | 0.7 | 0.75 | 0.28 | 0.62 | 0.82 | 0.60 |
| 13 | 0.3 | 0.3 | 0.3 | 0.85 | 0.33 | 0.5 | 0.96 | 0.52 |

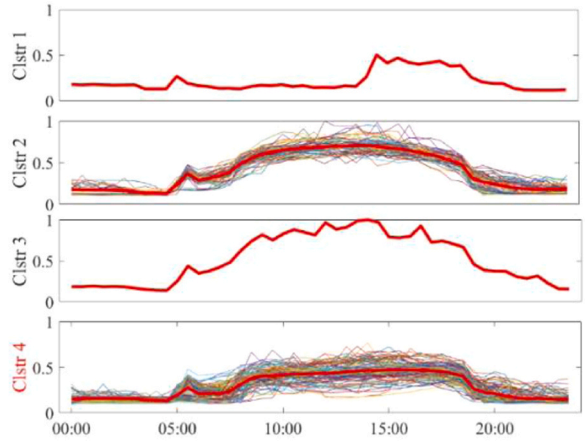


**Fig. 5.** The findings obtained through the clustering method developed for the summer group.

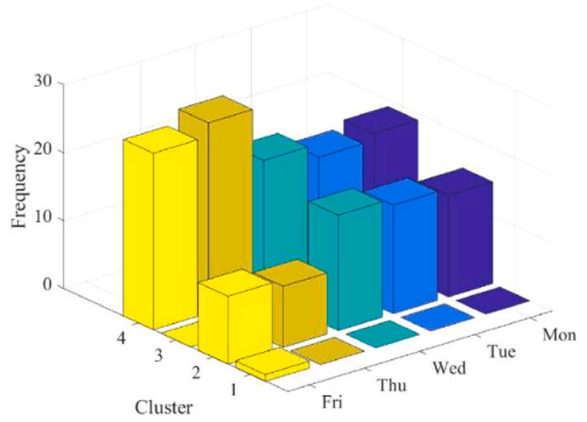


**Fig. 6.** The frequency distribution of each day within every cluster for the summer group.

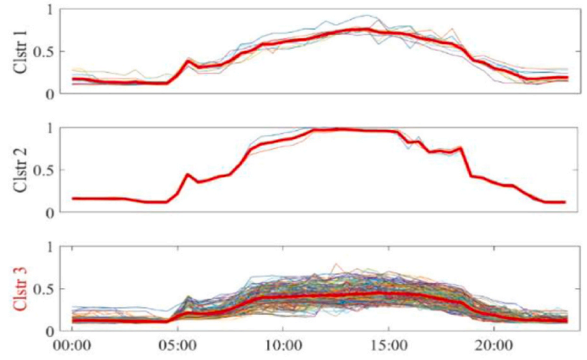


**Fig. 7.** The outcomes obtained from the clustering method developed for the Autumn group.

proposed problem. The modified IWO technique employs the wavelet mutation approach to prevent getting trapped in a local solution during the optimization process. The original and modified IWO techniques are described in the next sections.

### 3.2.1. Original IWO algorithm

IWO uses a population-based stochastic approach inspired by the behavior of the invasive weed colonies in agriculture (Mehrabian and Lucas, 2006). The initial population in this method is a generation

**Table 5**
The Clustering Results based On the Developed Framework for the Winter Group.

| Scenarios | Weights | | | Objective Functions | | | Criterions | |
|---|---|---|---|---|---|---|---|---|
| | w1 | w2 | w3 | Ob1 | Ob2 | Ob3 | DBI | SI |
| 1 | 1 | 0 | 0 | 0.77 | 0.38 | 0.5 | 1.73 | 0.40 |
| 2 | 0 | 1 | 0 | 0.88 | 0.44 | 0.37 | 1.47 | 0.41 |
| 3 | 0 | 0 | 1 | 0.93 | 0.77 | 0.12 | 1.44 | 0.32 |
| 4 | 0.7 | 0.3 | 0 | 0.88 | 0.62 | 0.37 | 1.54 | 0.37 |
| 5 | 0.5 | 0.5 | 0 | 0.90 | 0.46 | 0.5 | 1.53 | 0.30 |
| 6 | 0.3 | 0.7 | 0 | 0.92 | 0.43 | 0.62 | 1.58 | 0.19 |
| 7 | 0.7 | 0 | 0.3 | 0.89 | 0.58 | 0.5 | 1.38 | 0.37 |
| 8 | 0.5 | 0 | 0.5 | 0.89 | 0.62 | 0.25 | 1.41 | 0.37 |
| 9 | 0.3 | 0 | 0.7 | 0.93 | 0.68 | 0.12 | 1.25 | 0.42 |
| 10 | 0 | 0.7 | 0.3 | 0.98 | 0.56 | 0.25 | 1.65 | 0.34 |
| 11 | 0 | 0.5 | 0.5 | 0.95 | 0.65 | 0.25 | 1.47 | 0.33 |
| 12 | 0 | 0.3 | 0.7 | 0.89 | 0.74 | 0.12 | 1.45 | 0.35 |
| 13 | $0.\overline{3}$ | $0.\overline{3}$ | $0.\overline{3}$ | 0.82 | 0.67 | 0.12 | 1.06 | 0.56 |

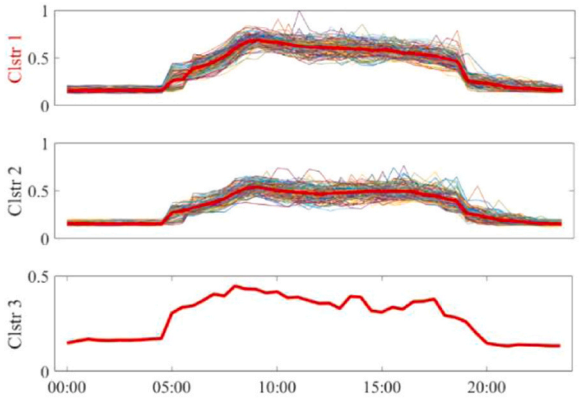


**Fig. 8.** The results stemming from the clustering method developed for the winter group.

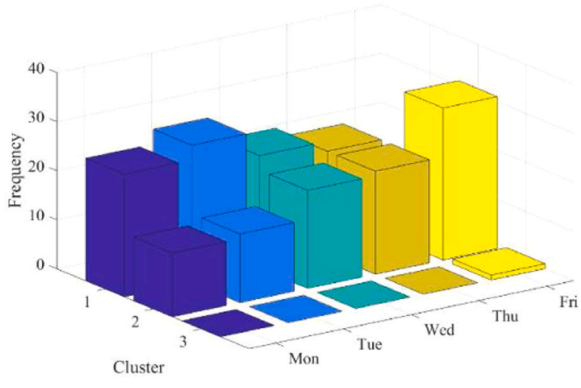


**Fig. 9.** The frequency distribution of each day within each cluster within the winter group.

placed randomly in the solution space like seeds in an agricultural field. The seeds are then ranked according to their fitness function to produce seeds again or for reproduction.

$$S_p = \left(\frac{S_{\max} - S_{\min}}{OF^{best} - OF^{worst}}\right) OF_p + S_{\min} \tag{13}$$

In this equation, $S_{\max}$ and $S_{\min}$ denote the predetermined maximum and minimum number of produced seeds, respectively; $OF^{best}$ and $OF^{worst}$ are the fitness functions of the best and worst population, respectively; $S_p$ and $OF_p$ signify the number of seeds generated by the $p^{th}$ seed and the

**Table 6**
Clustering Results of the Proposed Framework for the Holiday& Weekend Group.

| Scenarios | Weights | | | Objective Functions | | | Criterions | |
|---|---|---|---|---|---|---|---|---|
| | w1 | w2 | w3 | Ob1 | Ob2 | Ob3 | DBI | SI |
| 1 | 1 | 0 | 0 | 0.63 | 0.39 | 0.12 | 1.09 | 0.52 |
| 2 | 0 | 1 | 0 | 0.68 | 0.22 | 0.62 | 1.10 | 0.53 |
| 3 | 0 | 0 | 1 | 0.67 | 1 | 0 | 0.78 | 0.41 |
| 4 | 0.7 | 0.3 | 0 | 0.68 | 0.45 | 0.25 | 0.83 | 0.57 |
| 5 | 0.5 | 0.5 | 0 | 0.78 | 0.40 | 0.25 | 0.89 | 0.59 |
| 6 | 0.3 | 0.7 | 0 | 0.78 | 0.29 | 0.37 | 1.08 | 0.45 |
| 7 | 0.7 | 0 | 0.3 | 0.66 | 0.37 | 0.37 | 0.69 | 0.68 |
| 8 | 0.5 | 0 | 0.5 | 0.68 | 0.50 | 0.25 | 0.59 | 0.82 |
| 9 | 0.3 | 0 | 0.7 | 0.86 | 0.79 | 0.12 | 1.23 | 0.42 |
| 10 | 0 | 0.7 | 0.3 | 0.76 | 0.32 | 0.62 | 0.98 | 0.54 |
| 11 | 0 | 0.5 | 0.5 | 0.72 | 0.40 | 0.37 | 0.73 | 0.71 |
| 12 | 0 | 0.3 | 0.7 | 0.75 | 0.55 | 0.25 | 1.057 | 0.57 |
| 13 | $0.\overline{3}$ | $0.\overline{3}$ | $0.\overline{3}$ | 0.63 | 0.31 | 0.25 | 0.87 | 0.55 |

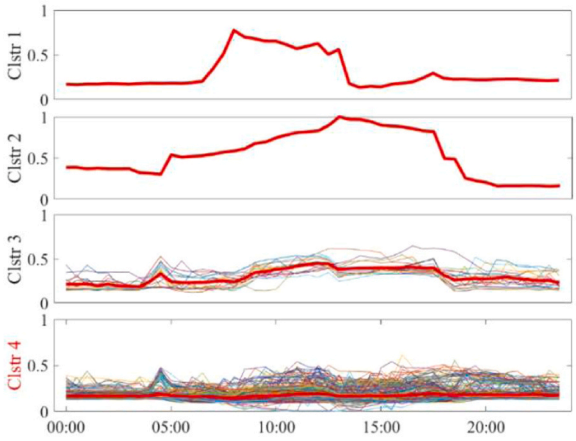


**Fig. 10.** The outcomes yielded by the clustering method developed for holidays and weekends.

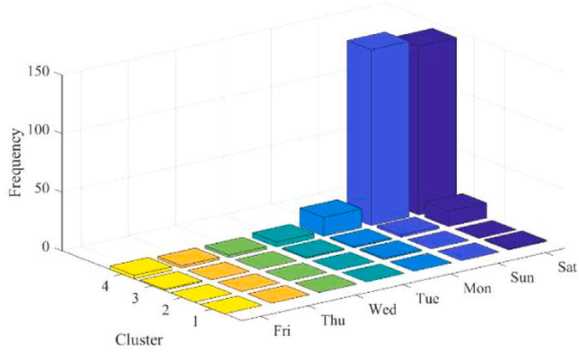


**Fig. 11.** The frequency distribution of each day within each cluster for the holiday and weekend group.

amount of fitness functions for the $p^{th}$ population.

In the subsequent stages, seeds are produced at random in the search space according to the normal distribution function, with the mean located at the mother plant position (original seed) and the standard deviation decremented as follows;

$$\sigma^{itr} = \sigma^{final} + \left(\frac{itr^{\max} - itr}{itr^{\max}}\right)^{\alpha} \left(\sigma^{initial} - \sigma^{final}\right) \tag{14}$$

where $\sigma^{itr}$ is the standard deviation at $itr^{th}$ iteration; $itr^{\max}$ is the maximum user-defined iteration; $\sigma^{final}$ and $\sigma^{initial}$ represent the final and initial standard deviations, respectively; and $\alpha$ is the nonlinear modulation index.

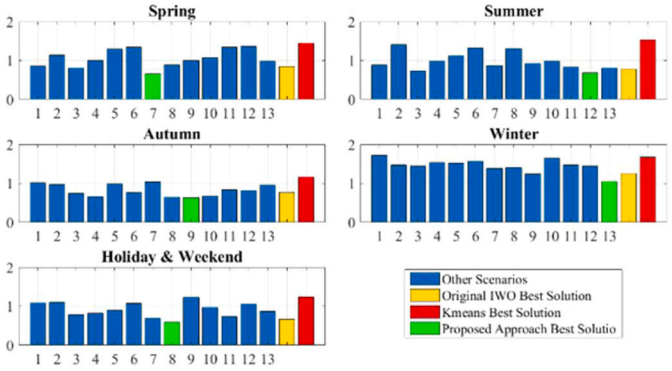


**Fig. 12.** The Davies-Bouldin metric score for different cases.

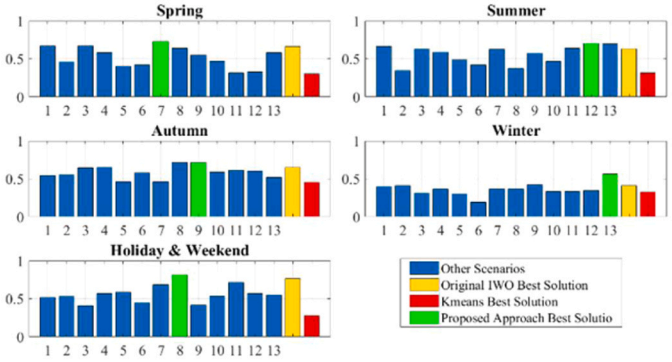


**Fig. 13.** The silhouette metric score for different cases.

Each of the original and new weeds are classified based on their fitness functions after reproduction. Weeds with poor fitness functions are eliminated and only a predefined number of them will remain for the next generation (iteration). These steps are repeated until the termination criterion is reached (i.e., the termination criterion is the maximum iteration).

### 3.2.2. Wavelet mutation strategy

A randomly chosen $p^{th}$weed and its $q^{th}$element will go through wavelet mutation at the ith iteration within the sorted population.

$$\Theta C_{p,q}^{itr} = \begin{cases} \Theta C_{p,q}^{itr} + \sigma\left(\Theta C_{q}^{\max} - \Theta C_{p,q}^{itr}\right), if & \sigma > 0 \\ \Theta C_{p,q}^{itr} + \sigma\left(\Theta C_{p,q}^{itr} - \Theta C_{q}^{\min}\right), if & \sigma \le 0 \end{cases} \tag{15}$$

Here $\Theta C_q^{\max}$and $\Theta C_q^{\min}$ respectively show the upper and lower bounds of for the $q^{th}$ component of the decision-variable vectors; $\sigma$ is the mother wavelet and calculated by;

$$\sigma = \Psi_{0,h}(r) = \frac{1}{\sqrt{h}} e^{-\frac{\left(\frac{r}{h}\right)^2}{2}} \cos\left(5\left(\frac{r}{h}\right)\right) \tag{16a}$$

$$s.t. h = e^{\left(\ln(h^{\max}) - \ln(h^{\max}) \times \left(1 - \frac{itr}{itr^{\max}}\right)^2\right)} \tag{16b}$$

where $r$ is a random integer produced from [− 2.5 h 2.5 h] and $h$ and $h^{\max}$are the dilation parameter and its maximum limit (i.e., $h^{\max}$= 10,000), respectively. In Bera et al (Bera et al., 2016)., more information regarding the wavelet mutation technique is given. Fig. 3 shows the

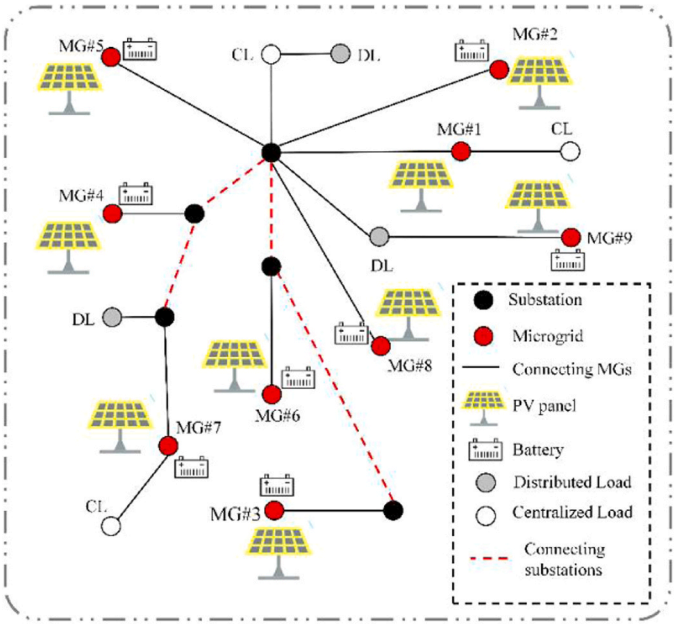


**Fig. 14.** The network representing the multi-microgrids system in this study.

structure of the suggested technique from solving the issue optimally.

### 3.2.3. Validity criterion for comparison

Two well-known matrices are employed to demonstrate the efficiency of the cluster for making an accurate comparison among the outcomes produced from the suggested technique and the results acquired from the standard k-means method. The Davies-Bouldin and silhouette indexes are the best metrics for indicating classification performance, as discussed in (Arbelaitz et al., 2013), and are thus utilized for comparing in this study. Arbelaitz et al (Arbelaitz et al., 2013). provide details on these indicators as well as additional metrics.

## 4. Results and discussion

### 4.1. The assessment of the clustering

The developed methodology is evaluated in this section using a genuine, typical load demand dataset of the WA facility. The data set covers three years of power use at a big local government's Civic Centre with a 30-minute time interval. At first, the suggested data is divided into five categories depending on dates: spring, summer, autumn, winter, and holiday and weekend combined. The recommended technique is then executed independently for every seasonal subgroup. The greatest and lowest number of clusters equals ten and two, respectively. The developed framework is carried out on a core-i7 laptop with a 2.8 GHz clock pulse and 16 GB of RAM by using the MATLAB software.

Table 1 provides the findings for the spring subgroup for 13 possible situations (i.e., various weight ratios). In addition, the values of the Davies-Bouldin and Silhouette indices (DBI and SI) are generated for each scenario in order to demonstrate the accuracy of clustering under each scenario and to choose the most suitable option. These findings demonstrate that the quantity of each objective function varies in relation to the weightings. The best DBI and SI values are found in the 7th Scenario (w1 =0.7, w2 =0, and w3 =0.3), which demonstrates that the dispersal measure does have the utmost ranking relative to the other metrics and the separation rate has the lowest priority. Furthermore, it was anticipated to contain a few clusters, and the majority of the observations would be anticipated to correspond to the identical cluster, which is supported by the clustering outcomes shown in Fig. 4.

**Table 7**
Comparison of the costs of the proposed energy sharing mechanism with the traditional scheme.

| Case | Collaborative | Non-Collaborative |
|---|---|---|
| MG1 Cost ($/year) | 182,062 | 187,172 |
| MG2 Cost ($/year) | 49,665.55 | 55,198.95 |
| MG3 Cost ($/year) | 15,355.55 | 15,746.1 |
| MG4 Cost ($/year) | 21,334.25 | 24,455 |
| MG5 Cost ($/year) | 31,240.35 | 37,222.7 |
| MG6 Cost ($/year) | 20,385.25 | 21,983.95 |
| MG7 Cost ($/year) | 15,103.7 | 16,260.75 |
| MG8 Cost ($/year) | 2620.7 | 3102.5 |
| MG9 Cost ($/year) | 3587.95 | 3942 |
| Total MGs Cost ($/year) | 341,355.3 | 365,084 |
| Energy loss (kWh/year) | 1,321,406 | 1,321,556 |
| Energy from upstream grid (kWh/year) | 21,203,887 | 21,224,206 |

Additionally, the majority of the days - all but one, "25-Nov-2016," belong to cluster two. All workdays of the week are represented by members of clusters two and three with roughly similar frequency. The percentage of every cluster in each group is displayed in Table 2. The table shows that the second category, which comprises more than 90% of the observations, is the dominating cluster.

For the other season categories, we also have equivalent outcomes and the same analysis. The 12th scenario in which the weighting factors (w1-w3) are set to 0, 0.3, and 0.7, respectively, to provide the best score for both DBI and SI, per the summer group's results in Table 3. In comparison to the number of clusters and the separation metric, which have higher priorities, the dispersion rate has the lowest priority. As a result, there are many clusters in the summer group, and the majority of the observations are associated with just a few clusters. In contrast, when w3 = 0.7, the number of clusters experienced their highest priority in the 9th scenario which is the best one for the fall group in Table 4 compared to the separation metric's lowest priority (w2 = 0) and the dispersion rate's highest value (w1 = 0.3). Since most of the observations would be anticipated to belong to the same cluster, it would be predicted that the autumn grouping had a limited range of clusters. According to Table 2, the final and second clusters that are represented in Fig. 5 contain about 62% and 37% of the observations in the summer group, correspondingly. Fig. 6 shows how often each day of the week occurs in every cluster.

This chart shows that cluster 4 includes the bulk of "Thursdays" and "Fridays." Conversely, the remaining days of the week were about equally distributed between clusters two and four.

The last cluster is home to about 94% of the observations in the fall group. Fig. 7 shows the results. To elaborate, just two days, "6th and 13th March of 2018″, are allocated to cluster two, the bulk of workdays are roughly equally distributed between clusters three and one, and Tuesday and Wednesday are representative of cluster one.

The winter group's results in Table 5 differ from those of the other categories. For the best case scenario (#13), the objective functions are prioritized equally, at 33% each. This indicates that the observations could be grouped into a few clusters with nearly equal proportions. Table 2 shows that 51.7% and 47.8% of observations are divided into two groups. Fig. 8 also depicts the clustering results of the ideal scenario in the winter season.

The weekly frequency of workdays for the winter category is shown in Fig. 9. It is clear that cluster two has the most "Fridays" allocated to it. Contrarily, the majority of "Mondays" and "Tuesdays" fall within cluster 1. The frequency of other days of the week is nearly alike in clusters one and two. Nearly identical to the fall grouping, the best case scenario (#8) for the holiday & weekend group in Table 6 has a greater priority (when weighting factors of objectives 1 and 3 equal to 0.5) in contrast to the separation metric which takes the least priority (weighting factor of

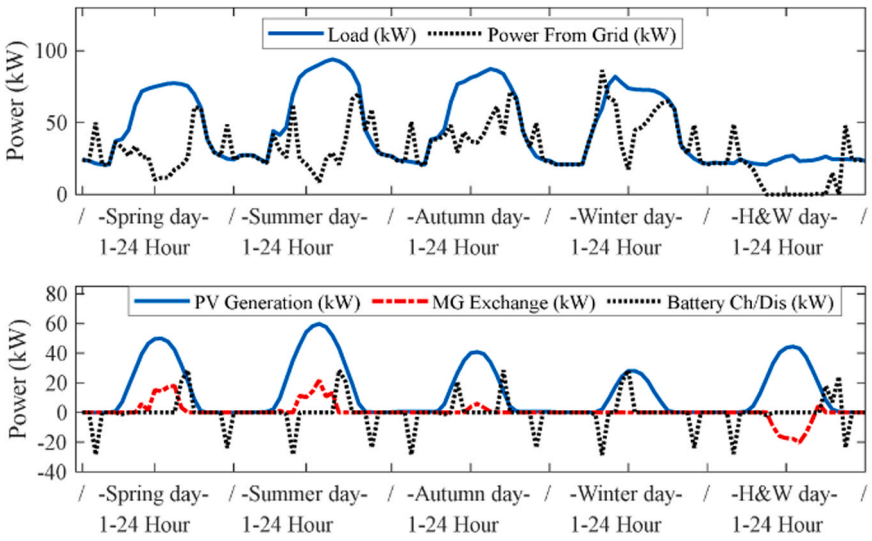


**Fig. 15.** The operational results of energy exchange between MG2 and the grid, as well as with other MGs, as determined by the proposed method, in comparison to MG2's load profile and PV output.

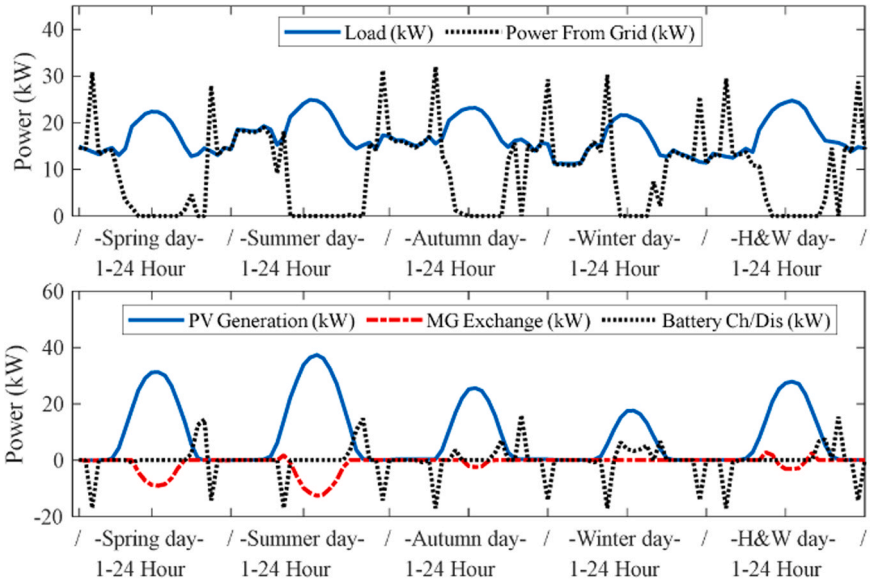


**Fig. 16.** The operational results of energy exchange with the grid and other MGs, as determined by the suggested method, in comparison to MG7's PV generation and load profile.

second objective function totalling 0). As a result, this group is likely to contain fewer clusters, and the majority of the observations correspond to the exact same cluster. Table 2 demonstrates that the last cluster may be allocated to more than 94% of the observations in this group. Fig. 10 depicts the outcomes of the proposed scenario. Furthermore, as shown in Fig. 11, the frequency of the holidays and weekend grouping is the same as in the dominant cluster.

The quantity of Davies-Bouldin and silhouette metrics for outcomes from the k-means technique, standard IWO, and all scenarios achieved by the proposed methodology are presented in Figs. 12 and 13, respectively, to demonstrate the superiority and efficacy of the framework. These numbers clearly demonstrate the improved effectiveness of the suggested technique, since the quantities for the two measures for all scenarios generated by the suggested methodology were superior to those derived from the standard and IWO k-means.

### *4.2. Assessing the Energy efficiency based on the results of clustering*

Load demand profiles over days offer helpful data associated with a facility that really can help with a study of its energy efficiency (Australian Government Department of Resources Energy and Tourism, 2023). The daily load profile might change daily or seasonally based on the facility type, the main demands, and the operational circumstances. Finding out what device is using energy when may be done by combining the daily load profile with a list of demands in the facility. This could then help in identifying areas where energy efficiency improvements and cost or energy reductions are possible.

Energy efficiency experts often examine the daily load demand over the period of a typical week for the four seasons of the year when researching buildings like commercial offices. This "average week" is typically selected as the season's midway week, eliminating any obvious outlier weeks, including those with public holidays or sporadic,

significant events. However, there is no inherent guarantee that the week picked will accurately reflect the average daily electrical load pattern for that season. The clustering method employed in this study ensures that the most representative daily load profiles are included in the analysis by providing a quantitative assessment of the representativeness of various daily load profiles. The findings indicate that, consistent with conventional wisdom, summer and winter are best described by two different profiles that, in the case of winter, happen nearly in a similar percentage. Spring, autumn, weekends, and public holidays may all be depicted by one profile.

The Civic Center facility analyzed in this paper has a load profile that is typical of most local government administration and civic center facilities. Due to the facility's mostly administrative use during regular business hours on weekdays, the load profile substantially corresponds to that of most commercial office buildings. Nevertheless, the load profile is diverse because periodically Civic Center activities—like council conferences and conventions place outside of regular business hours or on weekends and holidays (citizenship ceremonies, council functions or hiring of the hall facilities by the public).

The profile reveals that the heating, ventilation, air conditioning (HVAC) and lighting, which are turned on by the building's management system (BMS) at 4:30 AM and are turned off at 6:30 PM., are the main sources of energy use. The load increases from its overnight baseload rate in the morning to a significant quantity from 9:00 AM to 10:00 AM, then drops down to its overnight rate starting at 6:00 PM when the BMS turns off the lights and HVAC. Considering that HVAC and lighting are the principal loads, these are the primary areas on which examination of efficiency improvements should be concentrated.

In three seasons, specifically spring, autumn, and summer, there is a distinct spike from 4:30 to 5:30 AM, before the demand rises to its primary daylight level. This demonstrates that the BMS loses energy by operating when it is not necessary by not being designed to turn on the HVAC and lighting at the best time. Instead, during these months, it ought to be turned on a little later (nearer to 6:30AM), when it serves the primary load, which begins to increase around 8:30, and save about 2 h worth of electricity each weekday.

### 4.3. The results of planning of multi-microgrid systems

The example study includes nine MGs with installed solar and batteries, three centralized loads and three dispersed loads sites or nodes, each of which is situated in the centre of the grid. As seen in Fig. 14, all nodes are spatially dispersed over various regions. PV systems are modelled to have capacities of 100, 150, 96, 255, 13, 4.5, 94, 40, and 12 per kW for MG1 to MG9, respectively. Batteries for MG1 to MG9 have respectively the following capacities (kWh): 0, 57, 49, 58, 0.5, 1.5, 34, 12, and 9. Additionally, the load profiles of each MG and PV generation, which is dependent on solar radiation, have been grouped seasonally throughout a year as discussed in previous sections. The developed energy-sharing framework is implemented on the test case study (Fig. 14) under the following experiments to have a comprehensive comparison.

**Scenario1:** a cooperative/colaborative of MGs, which means MGs have active participation with each other, despite the communication with the grid.

**Scenario 2:** noncooperation/non-collaboration among MGs, meaning that there is no collaboration among MGs. In more detail, MGs merely interact with the grid by selling the excess power and purchasing the shortage of the power from the grid.

The findings of both mentioned scenarios are shown in Table 7. This table helps to easily compare the benefits of each method. Table 7 shows that the cost of each MGs in scenario 1, the cooperative mechanism, is less than the cost of the corresponding MGs with the non-collaborative mechanism. To illustrate that, the cost of MG2 ($/year) is 49,665.55 and 55,198.95 for collaborative and non-collaborative modes, respectively. In terms of the total cost ($/year), collaborative and non-collaborative are 341,355.3 and 365,084, respectively. From these comparisons, it can be seen that more cost reduction is obtained if the MGs collaborate with each other. This development in the case study demonstrates that there could be business potential if all local governments in Western Australia adopt the suggested plan over the time frame. Future funding to expand the use of renewable energy sources in local government buildings will also have a positive impact.

MG2 and MG7 have been chosen as illustrations to show the specifics of energy exchange amongst MGs. Figs. 15 and 16 depict the related demand and PV curves, their energy exchanges with the grid and other MGs, as well as the battery's state of charge. As can be seen, these two MGs function in various circumstances. For instance, MG2's PV production is lower than its demand, but MG7's PV production is more than its demand. MG2's demand also dramatically decreases during the holidays and weekends, although MG7's load is comparable to that of other clusters.

The outcomes vary for each MG as a result of these differences. In Fig. 15, MG2 purchases the electricity from other MGs in addition to deploying its own PV production to fulfill the demand. There remains a deficit, but it is being addressed by importing energy from the grid. The holiday and weekend cluster, meanwhile, is in a diverse set of circumstances because it can fulfill its demand and transfer any excess power to other MGs that require it (this cluster has negative values). In other words, when an MG sells its excess power to other MGs, the cost imposed on the receiving MGs is determined based on the levelized cost of energy (LCOE), and the network charge involved has a fixed daily component in addition to a variable one depending on the amount of energy exchanged. MG7 also uses its own PV production throughout the day, thus there is no need to import electricity from the grid, as shown in Fig. 16. The fact that MG7 cannot participate in energy sharing with other MGs in the fall and winter, when PV output declines, is also an intriguing observation.

## 5. Conclusion

In order to identify possible energy efficiency improvements, the power consumption characteristics of a facility can be successfully analysed through the clustering of load profiles. For long-term energy planning, realistic load profiles are also essential. The multi-dimensional approach of clustering that was devised and assessed in this work accounts for the dispersion within a cluster, the distance between clusters, and the total number of clusters. The clustering optimisation challenge has been addressed by developing and evaluating a novel hybrid technique that combines IWO and wavelet mutation algorithms. Three years' worth of half-hourly load data from a civic centre run by the local government were subjected to the clustering method. Clustered load profiles were created and analysed for every season, as well as for weekends and vacations. The results of the comparison of the novel clustering approach with the original IWO and well-known k-means clustering strategy demonstrate the superiority of the proposed methodology. By examining the clustered load profiles, an energy efficiency analysis of the local government facility was carried out. The analysis results demonstrate the effectiveness of the clustering strategy to help seize energy efficiency opportunities, such as effectively clustering load profiles with lower loads.

Additionally, a linear optimization approach for power sharing has been presented, allowing several MGs to trade energy with one another and/or the main network. The approach aids an organization that owns multiple MGs to efficiently trade and exchange electricity between its MGs and the main grid as necessary. The model solves the issue of when to trade with the network (both for the purchase and sale of energy), considering market pricing, and when and how much to trade with other MGs, considering the fee for network utilization, network charge, and loss. This optimization framework was applied and evaluated on a case study in WA consisting of a group of dispersed MGs with PV and energy storage systems controlled by a local (municipal) government. The

outcomes from the case study demonstrate that the operation costs are cheaper in the cooperative situation than in the situation when each MG interacts with the grid separately. Total MGs cost ($/year) for collaborative and non-collaborative conditions were 341,355 and 365,084, respectively. Similarly, the energy loss (kWh/year) associated with collaborative situations is 1,321,406, while it is 1,321,556 for the non-collaborative circumstance. These findings present a strong case for major organizations in WA to behave as retailers and include electricity trading among MGs as part of their energy management strategy. There is no doubt that each work has some advantages and limitations. Despite the advantages which have been discussed above, the limitation of this work would be associated with the load profile clustering. In order to improve the accuracy of operational planning, it is suggested that at least once a year, a new clustering is conducted to capture realistic patterns and changes of the load. This is not a very challenging task as the clustering, proposed in this paper, is run just once before handling planning optimization approach. For future work, the concept of a demand response program would be another strategy that could be integrated to increase the flexibility of the model.

## CRediT authorship contribution statement

Ali Azizivahed: Conceptualization, Methodology, Visualization, Investigation, Resources, Modeling and Simulation, Validation, Data Analysis, Main draft preparation. Khalil Gholami: Conceptualization, Methodology, Investigation, Main draft preparation. Gloria V. Rupf: Literature review and research gap finding, Data Analysis, Writing subsection 3.2. Ali Arefi: Supervision, Conceptualization, Writing subsection 2, Review-editing-feedback. Christopher Lund: Co-Supervision, Writing subsection 4.1, Review-editing-feedback. Jagpreet Walia: Data collection, Literature review and research gap finding. Moktadir Rahman: Data collection, Writing subsection 4.2, Review-editing-feedback. Rabiul Islam: Field data collection, Review-editing-feedback. Muyeen: Writing subsection 4.3, Review-editing-feedback. Innocent Kamwa: funding, Review-editing-feedback.

## Declaration of Competing Interest

The authors declare that they have no known competing financial interests or personal relationships that could have appeared to influence the work reported in this paper.

## Data availability

The data that has been used is confidential.

## Acknowledgment statement

This work was supported in part by the Canada National Sciences and Engineering Research Council through the Laval University, Grant ALLRP567550–21.

The authors wish to gratefully acknowledge funding for this research by the Australian Government Department of Industry, Innovation and Science under it's Smart Cities and Suburbs Program.

## References

Arbelaitz, O., Gurrutxaga, I., Muguerza, J., Pérez, J.M., Perona, I., 2013. An extensive comparative study of cluster validity indices. Pattern Recognit. 46 (1), 243–256. https://doi.org/10.1016/j.patcog.2012.07.021.

Arefi, A., Abeygunawardana, A., Ledwich, G., 2016. A new risk-managed planning of electric distribution network incorporating customer engagement and temporary solutions. IEEE Trans. Sustain. Energy PP (99), 1. https://doi.org/10.1109/TSTE.2016.2573290.

Australian Government Department of Resources Energy and Tourism, Energy Efficiency Opportunities Assessment Handbook," Commonw. Aust., no. ISBN 978–1-921812–58-3. (2023).

Azizivahed, A., et al., 2020. Energy management strategy in dynamic distribution network reconfiguration considering renewable energy resources and storage. IEEE Trans. Sustain. Energy 11 (2), 662–673. https://doi.org/10.1109/TSTE.2019.2901429.

Azizivahed, A., et al., 2021a. A multi-dimension clustering method for load profiles of Australian Local Government Facilities. 2021 IEEE 6th International Conference on Computing, Communication and Automation, ICCCA 2021. Institute of Electrical and Electronics Engineers Inc., pp. 819–825. https://doi.org/10.1109/ICCCA52192.2021.9666208

Azizivahed, A., Razavi, S.E., Arefi, A., Lund, C., 2021b. A Linear-based Model for Multi-Microgrid Energy Sharing- A Western Australia Case Study. in Proceedings of 2021 31st Australasian Universities Power Engineering Conference, AUPEC 2021. Institute of Electrical and Electronics Engineers Inc. https://doi.org/10.1109/AUPEC52110.2021.9597796

Bera, R., Mandal, D., Ghoshal, S.P., Kar, R., 2016. Wavelet Mutation based Novel Particle Swarm Optimization technique for comparison of the performance of single ring planar antenna arrays. in International Conference on Communication and Signal Processing, ICCSP 2016. Institute of Electrical and Electronics Engineers Inc., pp. 1659–1663. https://doi.org/10.1109/ICCSP.2016.7754445 (Nov.).

Castillo, C.A., Conde, A., Shih, M.Y., 2018. Improvement of non-standardized directional overcurrent relay coordination by invasive weed optimization. Electr. Power Syst. Res. 157, 48–58. https://doi.org/10.1016/j.epsr.2017.11.014.

Chicco, G., Ilie, I.S., 2009. Support vector clustering of electrical load pattern data. IEEE Trans. Power Syst. 24 (3), 1619–1628. https://doi.org/10.1109/TPWRS.2009.2023009.

Contreras, S.F., Cortes, C.A., Myrzik, J.M.A., 2019. Optimal microgrid planning for enhancing ancillary service provision. J. Mod. Power Syst. Clean. Energy 7 (4), 862–875. https://doi.org/10.1007/s40565-019-0528-3.

Deepak Sharma, D., Singh, S.N., 2014. Electrical load profile analysis and peak load assessment using clustering technique (Oct.). IEEE Power and Energy Society General Meeting. IEEE Computer Society. https://doi.org/10.1109/PESGM.2014.6938869.

Gholami, K., Jazebi, S., 2020a. Multi-objective long-term reconfiguration of autonomous microgrids through controlled mutation differential evolution algorithm. IET Smart Grid 3 (5), 738–748. https://doi.org/10.1049/iet-stg.2019.0328.

Gholami, K., Jazebi, S., 2020b. Energy demand and quality management of standalone diesel/PV/battery microgrid using reconfiguration. Int. Trans. Electr. Energy Syst. 30 (10), 1–21. https://doi.org/10.1002/2050-7038.12550.

Gholami, K., Karimi, S., Rastgou, A., 2022a. Fuzzy risk-based framework for scheduling of energy storage systems in photovoltaic-rich networks. J. Energy Storage 52, 104902. https://doi.org/10.1016/j.est.2022.104902.

Gholami, K., Abbasi, M., Azizivahed, A., Li, L., 2022b. An efficient bi-objective approach for dynamic economic emission dispatch of renewable-integrated microgrids. J. Ambient Intell. Humaniz. Comput. https://doi.org/10.1007/s12652-022-04343-5.

Gholami, K., Azizivahed, A., Arefi, A., 2022c. Risk-oriented energy management strategy for electric vehicle fleets in hybrid AC-DC microgrids. J. Energy Storage 50, 104258. https://doi.org/10.1016/j.est.2022.104258.

Gholami, K., Azizivahed, A., Arefi, A., Li, L., 2023. Risk-averse Volt-VAr management scheme to coordinate distributed energy resources with demand response program. Int. J. Electr. Power Energy Syst. 146, 108761 https://doi.org/10.1016/j.ijepes.2022.108761.

Haben, S., Singleton, C., Grindrod, P., 2016. Analysis and clustering of residential customers energy behavioral demand using smart meter data. IEEE Trans. Smart Grid 7 (1), 136–144. https://doi.org/10.1109/TSG.2015.2409786.

Khodaei, A., Bahramirad, S., Shahidehpour, M., 2015. Microgrid planning under uncertainty. IEEE Trans. Power Syst. 30 (5), 2417–2425. https://doi.org/10.1109/TPWRS.2014.2361094.

Kwac, J., Flora, J., Rajagopal, R., 2014. Household energy consumption segmentation using hourly data. IEEE Trans. Smart Grid 5 (1), 420–430. https://doi.org/10.1109/TSG.2013.2278477.

Li, R., Gu, C., Li, F., Shaddick, G., Dale, M., 2015. Development of low voltage network templates - part I: substation clustering and classification. IEEE Trans. Power Syst. 30 (6), 3036–3044. https://doi.org/10.1109/TPWRS.2014.2371474.

McLoughlin, F., Duffy, A., Conlon, M., 2015. A clustering approach to domestic electricity load profile characterisation using smart metering data. Appl. Energy 141, 190–199. https://doi.org/10.1016/j.apenergy.2014.12.039.

Mehrabian, A.R., Lucas, C., 2006. A novel numerical optimization algorithm inspired from weed colonization. Ecol. Inform. 1 (4), 355–366. https://doi.org/10.1016/J.ECOINF.2006.07.003.

Mets, K., Depuydt, F., Develder, C., 2016. Two-stage load pattern clustering using fast wavelet transformation. IEEE Trans. Smart Grid 7 (5), 2250–2259. https://doi.org/10.1109/TSG.2015.2446935.

Mina-Casaran, J.D., Echeverry, D.F., Lozano, C.A., 2021. Demand response integration in microgrid planning as a strategy for energy transition in power systems. IET Renew. Power Gener. 15 (4), 889–902. https://doi.org/10.1049/rpg2.12080.

Narayan, A., Ponnambalam, K., 2017. Risk-averse stochastic programming approach for microgrid planning under uncertainty. Renew. Energy 101, 399–408. https://doi.org/10.1016/j.renene.2016.08.064.

Narimani, A., Nourbakhsh, G., Arefi, A., Ledwich, G.F., Walker, G.R., 2019. SAIDI constrained economic planning and utilization of central storage in rural distribution networks. IEEE Syst. J. 13 (1), 842–853. https://doi.org/10.1109/JSYST.2018.2852630.

Piao, M., Shon, H.S., Lee, J.Y., Ryu, K.H., 2014. Subspace projection method based clustering analysis in load profiling. IEEE Trans. Power Syst. 29 (6), 2628–2635. https://doi.org/10.1109/TPWRS.2014.2309697.

Shawon, S.M.R.H., Liang, X., Janbakhsh, M., 2023. Optimal placement of distributed generation units for microgrid planning in distribution networks. IEEE Trans. Ind. Appl. 59 (3), 2785–2795. https://doi.org/10.1109/TIA.2023.3236363.

Tran, D., 2004. Fuzzy normalisation methods for pattern verification. Lect. Notes Comput. Sci. Incl. Subser. Lect. Notes Artif. Intell. Lect. Notes Bioinforma. 3072, 648–654. https://doi.org/10.1007/978-3-540-25948-0_88.

Wang, Y., Chen, Q., Kang, C., Xia, Q., 2016. Clustering of electricity consumption behavior dynamics toward big data applications. IEEE Trans. Smart Grid 7 (5), 2437–2447. https://doi.org/10.1109/TSG.2016.2548565.

Xu, Z., Yang, P., Zheng, C., Zhang, Y., Peng, J., Zeng, Z., 2018. Analysis on the organization and development of multi-microgrids. Renew. Sustain. Energy Rev. 81, 2204–2216. https://doi.org/10.1016/j.rser.2017.06.032.

Yang, J., Zhao, J., Wen, F., Dong, Z., 2019. A model of customizing electricity retail prices based on load profile clustering analysis. IEEE Trans. Smart Grid 10 (3), 3374–3386. https://doi.org/10.1109/TSG.2018.2825335.

Zhang, J., et al., 2016. A Bi-level program for the planning of an islanded microgrid including CAES. IEEE Trans. Ind. Appl. 52 (4), 2768–2777. https://doi.org/10.1109/TIA.2016.2539246.

Zhang, T., Zhang, G., Lu, J., Feng, X., Yang, W., 2012. A new index and classification approach for load pattern analysis of large electricity customers. IEEE Trans. Power Syst. 27 (1), 153–160. https://doi.org/10.1109/TPWRS.2011.2167524.